Organic/Inorganic Hybrids for Solar Energy Generation

Julia W.P. Hsu and Matthew T. Lloyd

Abstract

Organic and hybrid (organic/inorganic) solar cells are an attractive alternative to traditional silicon-based photovoltaics due to low-temperature, solution-based processing and the potential for rapid, easily scalable manufacturing. Using oxide semiconductors, instead of fullerenes, as the electron acceptor and transporter in hybrid solar cells has the added advantages of better environmental stability, higher electron mobility, and the ability to engineer interfacial band offsets and hence the photovoltage. Further improvements to this structure can be made by using metal oxide nanostructures to increase heterojunction areas, similar to bulk heterojunction organic photovoltaics. However, compared to all-organic solar cells, these hybrid devices produce far lower photocurrent, making improvement of the photocurrent the highest priority. This points to a less than optimized polymer/metal oxide interface for carrier separation. In this article, we summarize recent work on examining the polymer structure, electron transfer, and recombination at the polythiophene-ZnO interface in hybrid solar cells. Additionally, the impact of chemical modification at the donor-acceptor interface on the device characteristics is reviewed.

Introduction

Organic photovoltaics (OPVs) are targeted in small electronics, portable power, and integrated building applications because they are light weight, mechanically flexible, available in different colors, and compatible with roll-to-roll printing technologies for inexpensive manufacturing.[1,2] Most common OPVs consist of conjugated polymers as absorbing and donor materials (e.g., poly[3-hexylthiophene], P3HT) and fullerene derivatives (e.g., [6,6]-phenyl-C61-butyric acid methyl ester, PCBM) as acceptor materials. Presently, this materials system is capable of producing power conversion efficiencies (for areas ≥ 1 cm^2) of 4.4–5.0%.[3–5] By employing lower bandgap donor materials and utilizing a C_{70} derivative as an acceptor, certified power conversion efficiencies above 7.4% for a small area sample (~0.1 cm^2) have been achieved.[6] Increased power conversion efficiency and device stability are the two most critical issues for OPVs to fully realize their technological viability.

Hybrid devices that combine organic and inorganic semiconductors show promise in achieving unique functionalities that cannot be obtained for each component alone. In energy utilization, applications spanning from light-emitting devices[7,8] to energy conversion[9,10] have been explored. For polymer solar cells, the substitution of oxide semiconductors (e.g., ZnO or TiO_2) for fullerenes as the electron acceptor and transporter has the advantage of better environmental stability,[11–14] higher electron mobility, and the ability to engineer interfacial band offsets and hence the photovoltage.[15,16] The electron affinity of ZnO and TiO_2 provides the suitable band alignment for charge transfer from the lowest unoccupied molecular orbital of the donor polymer to the conduction band of the metal oxide acceptor. Further improvement to this structure can be made by creating mesoporous structures of the metal oxide into which the conjugated polymer can be infiltrated.[17,18] In particular, ZnO nanostructures can be synthesized with a variety of growth and processing methods, including vapor deposition,[19–21] solution-based crystal growth,[22–26] spray pyrolysis,[27] and conversion from a precursor source in the polymer matrix.[28,29] To date, even with improved architecture, hybrid solar cell efficiencies remain well below those achieved in the pure organic systems. Hence, interfacial studies of structural, chemical, and electronic properties in the polymer/metal oxide systems are critical in advancing this field.

As an introduction to hybrid solar cells, we first consider simple bilayer architectures as shown in Figure 1: (a) a cross-sectional schematic and (b) a cross-sectional transmission electron microscopy image of a P3HT/ZnO bilayer solar cell. In hybrid photovoltaic devices, light absorption occurs in the conjugated polymer, resulting in bound electron-hole pairs (excitons). The excitons then dissociate to

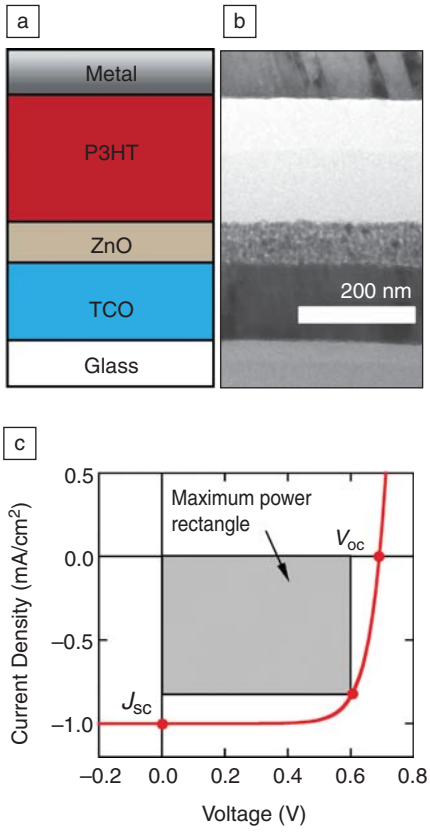

Figure 1. (a) Schematic and (b) transmission electron microscopy image for a P3HT/ZnO bilayer hybrid photovoltaic device architecture in cross section. (c) Example of current-voltage characteristics for a photovoltaic device under illumination. V_{oc} and J_{sc} are the open-circuit voltage and short-circuit current density, respectively. The maximum power this solar cell can deliver is represented by the gray shaded region. The power conversion efficiency is the ratio of this area to the incident of light power density. TCO, transparent conducting oxide.

form free carriers, with electrons being transferred to the inorganic acceptor materials and the holes remaining in the polymer (see the article by Zhu and Kahn in this issue). Due to the lattice distortions accompanying the charges in organic materials, charge carriers in the polymer are called polarons. The separated electrons and holes can transport to their respective electrodes and generate photocurrent or recombine across the interface without generating photocurrent. Hence, the performance of these solar cells critically depends on the electron transfer and recombination at the organic/inorganic heterojunction interface. In this type of solar cell, the transparent conducting electrode, typically indium tin oxide or fluorine-doped tin oxide, collects the photo-generated electrons while the top metal electrode, typically silver or gold, collects the photo-generated holes. Figure 1c depicts a current-voltage curve of a solar cell and definition of device parameters. The current density at zero bias is called the short-circuit current density, J_{sc}. The voltage at which there is no net current (i.e., the photocurrent exactly cancels the dark current) is called the open-circuit voltage, V_{oc}. The power conversion efficiency (PCE) of the solar cell is the product of V_{oc}, J_{sc}, and FF (fill factor) (shaded area in Figure 1c) divided by the incident power density, where FF is the ratio of the shaded area to the rectangular area given by V_{oc} times J_{sc}. To date, the PCE of hybrid solar cells falls short of the requirements for commercial exploitation, in large part due to low short-circuit currents.[18,30] While the bulk energy levels of the inorganic acceptor materials indicate an energy offset that is sufficient to dissociate excitons, equivalent all-organic bilayer devices (utilizing a fullerene acceptor)[31,32] produce photocurrents five to 10 times higher than similar hybrid devices.[33] Thus, factors that affect charge transfer efficiency and subsequent recombination at the polymer/metal oxide interface are critical issues, and they are currently not well understood.

Modification of the interface between the metal oxide and the polymer to enhance exciton dissociation and charge transfer has been recently pursued. These interfacial modification studies commonly utilize a simple bilayer device architecture (Figure 1a), where the donor-acceptor interface is modified with an organic layer[33–35] or with conformal inorganic coatings.[36,37] Interestingly, while the organic modifiers generally have little effect on the device open-circuit voltage V_{oc},[33,35,38–40] the inorganic modifiers significantly increase V_{oc}.[36,37] In this article, we review studies that elucidate the causes responsible for the low photocurrent in hybrid solar cells. These studies also explain the mechanisms behind improved photovoltaic device performance when employing an alkanethiol self-assembled monolayer (SAM) at the P3HT/ZnO interface. This finding has significant implications for hybrid device design and highlights the importance of interactions between donor and acceptor materials at the heterojunction interface.

Interfacial Polymer Morphology: Effect of Substrate Interaction

P3HT is the commonly used semiconducting polymer in OPVs and is exclusively used in hybrid solar cells due to its tendency to organize into microcrystalline domains, which are responsible for high hole mobility.[41–43] However, the formation of P3HT crystalline domains, and consequent impact on device performance, is extremely sensitive to material properties (e.g., regioregularity or molecular weight),[44,45] processing conditions (e.g., solvent, annealing temperature, or spin coating speed),[46–49] and substrate surface chemistry.[50]

Recent results suggest that in P3HT/ZnO hybrid solar cells, the P3HT in immediate contact with ZnO might be disordered. This is consistent with both the blueshift in the absorption and photoluminescence spectra observed for thin (<10 nm) P3HT films deposited on ZnO[33,51] and in the spectra of photocurrent yield[30] and microwave conductivity yield[52] of P3HT/ZnO nanoparticle composite solar cells. Disordered interfacial P3HT reduces overlap with the solar spectrum and decreases exciton diffusion and hole transport within the polymer,[53,54] resulting in poor photovoltaic performance. Furthermore, the energy level positions of relevant molecular orbitals are likely to be different for ordered and disordered polymers,[55] which would affect electron transfer at the P3HT/ZnO interface. In this section, we first summarize results obtained using different techniques to establish an amorphous P3HT layer at the ZnO interface. Next we show an example of modifying the surface ZnO films with an alkanethiol SAM that restores the ordering in the interfacial P3HT layer, leading to an improvement in J_{sc}.

Optical and Structural Properties of Thin Polymer Films

Figure 2a displays the normalized absorption spectra of thin P3HT films on glass, a ZnO sol-gel film, and a hexadecanethiol-modified ZnO sol-gel film. The absorption spectrum of the neat P3HT film on glass (black curve) clearly shows three features associated with regioregular P3HT at 525, 566, and 610 nm. It was shown that the two lowest energy features are extremely sensitive to the ordering of the polymer.[56–58] Hence, their presence signifies enhanced polymer ordering in the film. When P3HT is deposited on ZnO (red curve in Figure 2a), the main absorption peak shifts to a shorter wavelength and does not show these low-energy

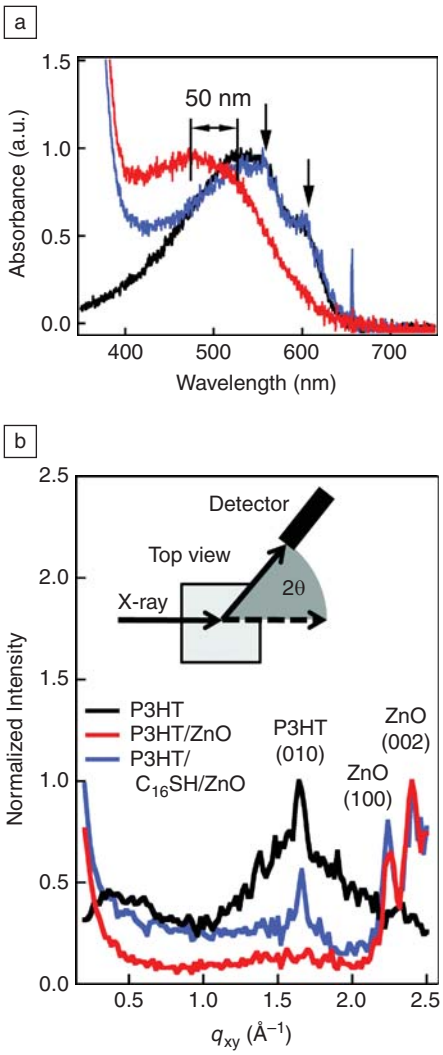

Figure 2. (a) UV-vis absorption spectra of thin P3HT films (~6 nm) deposited on glass (black), unmodified ZnO (red), and hexadecanethiol-modified ZnO (blue). (b) Grazing incidence x-ray diffraction (GIXD) spectra for thin P3HT films (<10 nm) deposited on the substrates designated in (a). The magnitude of the in-plane scattering vector is q_{xy}. The inset shows the GIXD geometry for x-rays collected over diffraction angle 2θ. Reprinted with permission from Reference 29. ©2009, Royal Society of Chemistry.

structures, suggesting the existence of a disordered P3HT layer.

To directly measure the structure of the P3HT film, an in-plane grazing incidence x-ray diffraction (GIXD) experiment was performed. As shown in Figure 2b, the salient feature for a P3HT film on glass (black curve) is a diffraction peak at 1.64 $Å^{-1}$ emerging from a broad scattering background. For a grazing-incidence scan, the location of this peak indicates that the (010) direction (the polymer interchain π-stacking direction) of the P3HT domains is aligned parallel to the substrate, consistent with published results.[4,41] Given the lack of diffraction signal for the 0.39 $Å^{-1}$ reflection (P3HT (010) peak), these in-plane diffraction results indicate little out-of-plane π-stacking (i.e., few domains align with the (100) direction oriented parallel to the substrate). This is typical of highly ordered regioregular P3HT films.[4,54,59]

In stark contrast, P3HT deposited on ZnO (Figure 2b, red curve; the blue curve is discussed in the next section) shows a conspicuous absence of any polymer lattice peaks and displays only the ZnO crystallographic peaks. The lack of P3HT lattice peaks confirms the hypothesis that the blueshift observed in the absorption spectrum originates from amorphous P3HT formed within the first few nanometers of the ZnO surface. Annealing is often employed to increase the size and number of crystalline domains of P3HT in bulk heterojunction solar cells.[4] When the polymer-substrate interaction is low, as in the case of P3HT on glass, an annealing treatment imparts sufficient conformational mobility for P3HT to adopt preferentially oriented domains.[54] The fact that these annealed films on ZnO remain amorphous provides unequivocal evidence that the substrate interaction has a large effect on the morphology of the interfacial P3HT layer. Note that this change in the absorption spectra can only be observed if the P3HT film thickness is less than 10 nm. For thick films (80–100 nm) that are employed in the solar cells, the spectra on glass and on ZnO are identical, indicating only the interfacial P3HT layer is sensitive to the substrate interaction. The use of very thin (~6 nm) P3HT films to model the interfacial polymer layer enables us to probe the changes at the interface.

Having consistently observed a change in the absorption spectrum, what is the origin of disorder P3HT interfacial layers on ZnO? In dispersed ZnO nanoparticle/P3HT heterojunctions, it has been suggested that the conformation of polythiophene chains deviate from planarity when in close proximity to ZnO nanoparticles, which, in turn, reduces the conjugation length of P3HT.[52] Given that the sol-gel-derived ZnO surface is essentially flat (3 nm root mean square roughness as measured by tapping mode atomic force microscopy), disruption of polymer order due to the curvature of the ZnO surface cannot be the primary source of morphological disordering when P3HT is deposited on sol-gel ZnO films. Zn–S bond energy is quite high (205 kcal/mol),[60] which suggests strong interaction between ZnO and P3HT, leading to immobilization of P3HT and an amorphous morphology. Thus, substrate chemistry plays a more important role, similar to that previously reported on modified silicon oxide surfaces.[44]

Interfacial Modification with Alkanethiol Monolayers

To improve the electron transfer efficiency at the donor-acceptor interface, introducing a monolayer of organic molecules at the interface has been explored to alter the energy band alignment through the introduction of interfacial dipoles[34] or to add electron acceptors with intermediate energy levels.[35] Here we discuss results of using an organic SAM to modify surface chemistry, hence the surface energy. Alkanethiol SAMs of different hydrocarbon chain lengths ($CH_3(CH_2)_nSH$, n = 3 to 17) were deposited on the ZnO surface in ZnO/P3HT bilayer photovoltaic devices. Alkanethiols are chosen because they readily form monolayers on ZnO surfaces through Zn–S bonding and are available in incrementally increasing lengths.[33]

As discussed previously, thin P3HT films deposited on ZnO exhibit an amorphous structure. The effect of an alkanethiol SAM-modified ZnO surface on a P3HT structure is shown by the absorption data presented in Figure 2a (blue curve) and Figure 3. The absorption spectra of P3HT deposited on the modified surfaces depend on the length of the molecule: the longer the alkanethiol molecule, the less the blueshift (Figure 3 inset) and the more the absorption spectrum resembles P3HT on glass. The blueshift is reduced from over 50 nm on ZnO to 6 nm on octadecanethiol-modified ZnO. The low-energy absorption features also are recovered, indicating that P3HT films deposited on alkanethiol-modified ZnO are more ordered. The in-plane GIXD spectrum (Figure 2b blue curve) confirms that P3HT deposited on alkanethiol-modified ZnO is indeed ordered. In addition to diffraction peaks from the ZnO substrate, the P3HT (010) direction scattering peak returns at 1.64 $Å^{-1}$, although with slightly diminished intensity compared to P3HT on glass (Figure 2b black curve). Like on glass, P3HT on the alkanethiol-modified ZnO surface displays preferential alignment of the in-plane π-stacking direction.

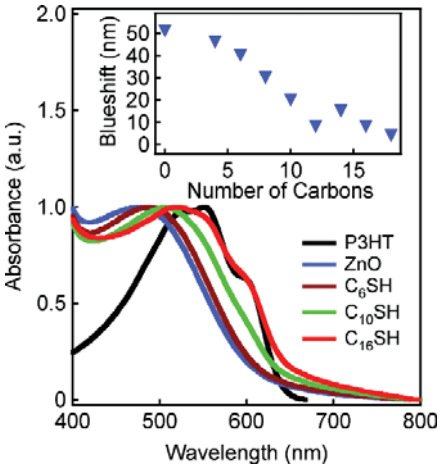

Figure 3. UV-vis spectra of P3HT on alkanethiol-modified ZnO substrates. Inset: Magnitude of blueshift in the absorption spectra as a function of alkanethiol chain length. Reprinted with permission from Reference 18. ©2008, Wiley.

Surface energy measurements show that alkanethiol SAMs dramatically reduce the ZnO surface energy by a factor of 2 to 3, monotonically with the molecular chain length. Thus, P3HT polymers are more mobile on the alkanethiol-modified surface during annealing and can re-order to form larger domains.[54] Recently, Peet et al. reported that the addition of alkanethiol or alkanedithiol to P3HT solutions promotes structural order due to slow crystallization.[61] It is possible that the alkanethiol bound to the ZnO surface has a similar effect on P3HT crystallization kinetics. This is a clear example of polymer-substrate interaction: the polymer physical property can be tuned through the incorporation of an interfacial layer.

Impact on Solar Cell Devices

To investigate the effect of alkanethiol modification on solar cell performance, bilayer devices made using unmodified ZnO and alkanethiol-modified ZnO films are compared. Figure 4a shows the current density versus voltage (*J-V*) curves for an unmodified ZnO, decanethiol ($C_{10}SH$), and octadecanethiol ($C_{18}SH$)-modified ZnO illuminated under a simulated terrestrial one sun condition, while the inset shows *J-V* curves for the same devices in log-linear scale taken without light. Table I summarizes the device characteristics (J_{sc}, V_{oc}, FF, PCE, series and shunt resistance) for these devices. The general findings are (1) the series resistance increases with increasing molecular length; (2) V_{oc} is unaffected by the alkanethiol modification; and (3) J_{sc} increases as molecular length increases.

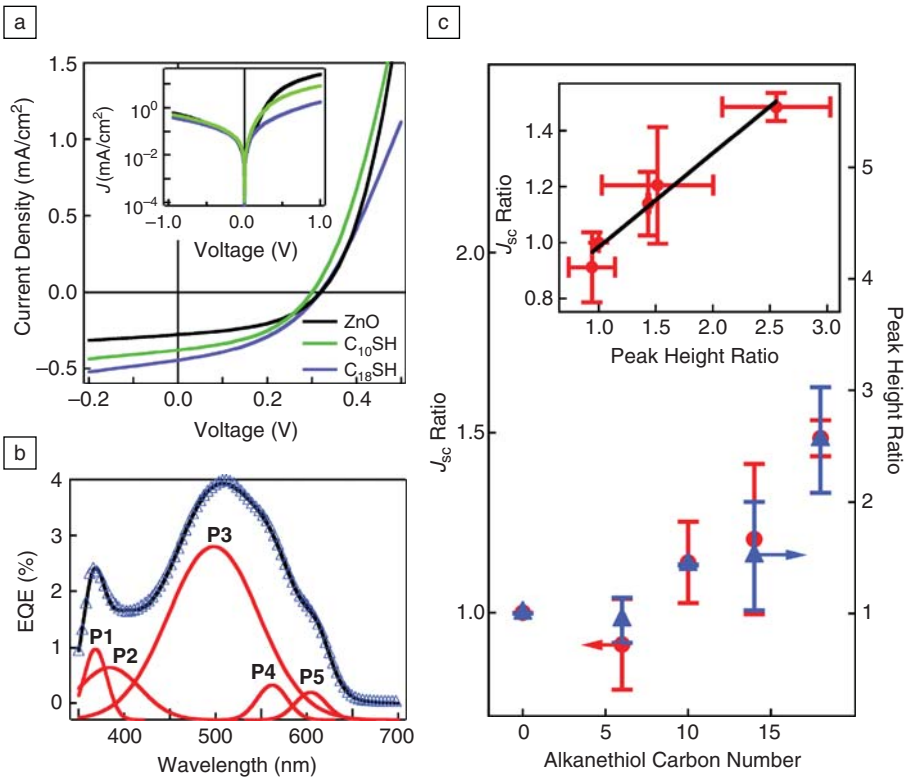

Figure 4. (a) Current density-voltage characteristics for P3HT-modified ZnO devices with 100 mW/cm² illumination intensity. Inset: Current-voltage characteristics in the dark. (b) Multipeak fit for a C_{18}SH-modified device to analyze the blueshift and degree of P3HT ordering reflected in the external quantum efficiency (EQE). The blue triangles are the experimental data. The red curves (P1 through P5) are the five peaks used for the fitting, with four long wavelength peaks representing P3HT, and the peak at 366 nm representing ZnO. The black curve is the sum of all the red curves. (c) Short-circuit photocurrent J_{sc} and EQE peak height ratio as a function of alkanethiol chain length. Inset: Linear correlation between the J_{sc} ratio and the EQE peak height ratio. Reprinted with permission from Reference 18. ©2008, Wiley.

Table I. Current-Voltage Characteristics for Unmodified, C_{10}SH, and Modified, C_{18}SH, Devices.

Sample	J_{sc}[a] (mA/cm²)	V_{oc} (mV)	Fill Factor	PCE (%)	R_{series}[b] (Ω cm²)	R_{shunt}[c] (kΩ cm²)
Unmodified	0.28 ± 0.011	305 ± 15	42.7 ± 2.7	0.037 ± 0.004	27 ± 3	2.9 ± 0.7
C_{10}SH	0.35 ± 0.021	290 ± 9	43.1 ± 1.8	0.043 ± 0.004	41 ± 2	1.6 ± 0.2
C_{18}SH	0.42 ± 0.020	312 ± 5	40.4 ± 0.8	0.053 ± 0.003	98 ± 5	2.0 ± 0.1

[a]All values are the average of six devices; ± represents the standard deviation.
[b]Series resistance measured under illumination at 1 volt forward bias.
[c]Shunt resistance measured in the dark with zero applied bias.
J_{sc}, short-circuit current; V_{oc}, open-circuit voltage; PCE, power conversion efficiency; R_{series}, series resistance for unmodified devices; R_{shunt}, shunt resistance for unmodified devices.
Reprinted with permission from Reference 18. ©2006, Elsevier.

It is expected that alkanethiol SAMs will increase the series resistance, since they are insulating and present a tunneling barrier in the device. This expectation is supported by the increasing series resistance with increasing alkanethiol molecular length. Hence, one might expect that photocurrent would also be reduced because of the presence of an alkanethiol SAM tunneling barrier for electrons. Quite oppositely, the J_{sc} of these devices shows a clearly increasing trend with the alkyl chain length of the modifying alkanethiol monolayers. The J_{sc} increase is also reflected in the external quantum efficiency (EQE) spectrum (Figure 4b), which measures the number of photogenerated carriers extracted from the device divided by the number of incident photons. Since only the separated photogenerated charges, with electrons transferred to the ZnO, contribute to the EQE signal, EQE is sensitive to the polymer layer within an exciton diffusion length (<10 nm) of the interface. The low-energy features are visible in the EQE spectrum of the C_{10}SH-modified device and prominent in the C_{18}SH-modified device (Figure 4b), similar to the absorption spectra of thin P3HT films on these modified ZnO surfaces.[33] Thus, alkanethiol modification results in increased ordering of the interfacial P3HT layer, as is evident in the GIXD spectra and in the pronounced low-energy features in the absorption and EQE spectra; consequently, the J_{sc} in the solar cells is enhanced.

To quantitatively analyze the structural change with the J_{sc} increase, the EQE spectra were fitted with five peaks, labeled P1 through P5 in Figure 4b.[33] Figure 4b shows the EQE spectrum and the peaks used to fit the spectrum for the C18SH-modified devices. To quantify the contribution from enhanced structural order, the heights of two low-energy peaks (P4 and P5 in Figure 4b) were summed for alkanethiol-modified devices and normalized to those for the unmodified device fabricated in the same batch. Similarly, the average J_{sc} for a modified sample is divided by that for an unmodified sample fabricated in the same batch. This ratio quantifies the relative increase in the J_{sc} over an unmodified sample. Figure 4c depicts the correlation between the increases in the J_{sc} and the intensity of the two low-energy EQE peaks with molecular length for all devices. Both J_{sc} and the interchain contribution to the EQE increase as the alkyl chain length increases, and the two are also strongly correlated (Figure 4c inset).[33]

Photoexcitation Dynamics

The previous section shows that the morphology of the interfacial polymer layer is strongly disordered due to its interaction with the ZnO substrate, and by inserting an alkanethiol SAM at the interface, the P3HT ordering is restored. As discussed in the previous section, the solar cells with more ordered P3HT interfacial layers generate higher photocurrent despite the charge transfer barrier presented by the insulating SAM. Transient photo-induced absorption (TPA) is a spectroscopic technique that measures

sub-bandgap absorption of photoexcited species, such as polarons and excitons, as illustrated in Figure 5a.[62] The TPA signal ($-\Delta T/T$) monitors the change in transmission through the sample due to photoexcitation as a function of the delay between the excitation pulse and the probe. To directly compare the yield of photoexcited species in different samples, the optical density of the film at the excitation wavelength (550 nm) is used to normalize the TPA signal (Figure 5b). From spectrally resolved TPA data, we can identify the type of photoexcited species by the energy of its characteristic optical transition. The dynamics of the signal at a specific energy provides information on the lifetime of the species. By directly measuring photoexcitation dynamics and the recombination of photoexcited species using TPA, we can gain a better understanding of the mechanism(s) behind photocurrent enhancement, even in the presence of a tunneling barrier (discussed previously).

Spectroscopy of Polarons and Excitons

Figure 5b shows the TPA signal at $t = 0$ for both P3HT on glass and P3HT/ZnO composite films for probe energies between 0.41–1.14 eV. Distinct absorption peaks arise at ≤ 0.41 (P_1), 0.92 (PA_1), and 1.14 (P_2) eV for both P3HT on glass and the P3HT/ZnO composite. The TPA peak P_1 at ≤ 0.41 eV is assigned to low-energy polaron absorption with a great degree of certainty due to the fact that polarons are the only absorbing species in the 0.3–0.5 eV vicinity.[63] Photo-induced absorption peaks PA_1 (0.92 eV) and P_2 (1.14 eV) are assigned to exciton and higher energy polaron absorptions, respectively, based on recent TPA studies of regioregular P3HT.[62] The most striking observation seen in Figure 5b is the similarity between the TPA spectra for P3HT on glass and the P3HT/ZnO composite. The magnitude of the TPA signal at $t = 0$ reflects the initial concentration of the photoexcited species. The signals for P3HT on glass are from excitons and polarons photo-generated in the neat film. Exciton dissociation efficiency in regioregular P3HT is high compared to other conjugated polymers.[62] Hence, polarons can be generated in P3HT films without an acceptor nearby. In a donor-acceptor system with efficient charge transfer, polaron signals would be larger than the neat film as a result of additional exciton dissociation at the interface and electron transfer into the metal oxide. For example, in bilayers of P3HT/nanocrystalline SnO_2, ultrafast pump-probe measurements showed that the $t = 0$ signal for polarons is larger by a factor of six compared to neat films of P3HT.[64] In contrast, the $t = 0$ concentration measured in P3HT/ZnO composite is remarkably similar to P3HT on glass. Furthermore, P_2 shows a measurably larger initial polaron concentration in P3HT on glass. These results indicate that ZnO is not effective in promoting exciton dissociation at the interface on the picosecond timescale.

Decay Dynamics of Polarons and Excitons

The time dependence of TPA signals provides information on the decay dynamics of the polarons and excitons in different samples. The data show a multi-exponential decay behavior for all three photoexcited species over a period of 0–500 ps. Since the rise time for all species and all samples are the same, 200 ± 15 fs, the TPA behavior is dominated by recombination processes over the first 500 ps. Figure 5c compares weighted average lifetimes for the three photoexcited species (P_1, PA_1, and P_2) in P3HT on glass, P3HT/ZnO composite bilayer, and P3HT on C_{16}SH-modified ZnO samples. It is evident that the lifetimes of all photoexcited states in the P3HT/ZnO bilayer are measurably lower than in the other samples.[51] As discussed previously, in the case of efficient exciton dissociation (followed by charge separation), a stabilized polaron population (i.e., longer lifetime) is expected to form in the P3HT/ZnO composite sample resulting from electron transfer into ZnO. For P3HT on glass, we would expect to see faster polaron recombination because the generated negative charges remain in P3HT readily available to recombine with the positive polarons. Instead, we see more rapid decay or higher recombination rates for all three photoexcited species in the P3HT/ZnO composite. Since P3HT on ZnO is amorphous while the other two samples are partially ordered, it appears that polymer morphology has the largest effect on the lifetimes of photoexcited species. The weighted average exciton (PA_1) lifetime of the two ordered P3HT samples (on glass and C_{16}SH-modified ZnO) is approximately the same, further indicating that ordered materials have fewer recombination centers. In addition, the low- and high-energy polarons (P_1 and P_2) exhibit a measurably longer lifetime in the C_{16}SH-modified ZnO sample than in the glass sample. Such an increase in the polaron lifetime (not the number of polarons at $t = 0$ s) demonstrates lower recombination rates in the C_{16}SH-modified ZnO sample and possibly demonstrates enhanced charge separation between ZnO and P3HT and reduced recombination.

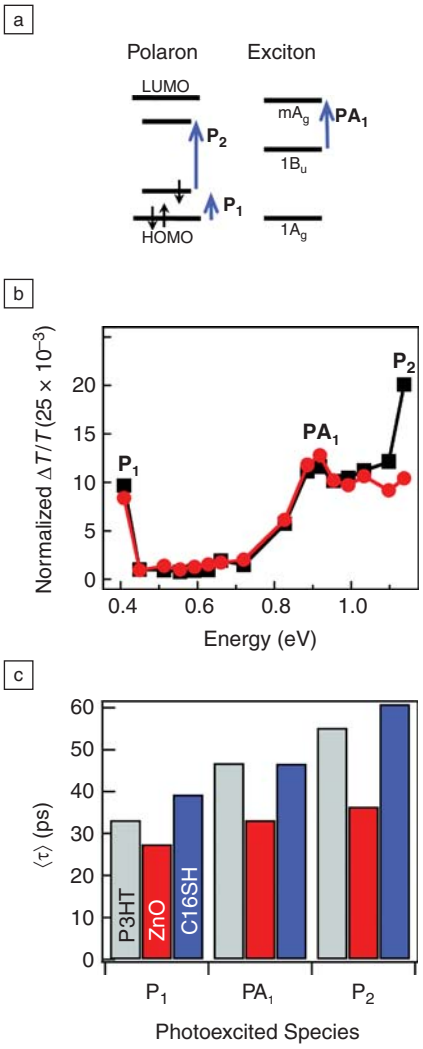

Figure 5. (a) (Left) Molecular electronic energy level diagram showing optical transitions (P_1 and P_2) for polaron states that give rise to sub-gap absorption indicated in (b). (Right) Neutral exciton manifold indicating the optical transition (PA_1) for the first excited state of the lowest-lying singlet exciton.[62] (b) Transient photo-induced absorption signal at time $t = 0$ as a function of probe energy for P3HT on glass (black) and on unmodified ZnO (red). To account for variation in film thickness, the transient photo-induced absorption signal ($-\Delta T/T$) has been normalized by the optical density of the polymer at the excitation wavelength (550 nm). (c) Weighted average lifetime for each photoexcited species in P3HT on glass (gray), the P3HT/ZnO composite (red), and the P3HT/C16SH/ZnO composite (blue). HOMO, highest occupied molecular orbital; LUMO, lowest unoccupied molecular orbital. Reprinted with permission from Reference 29. ©2009, Royal Society of Chemistry.

The fact that the TPA spectra and decay dynamics are similar for P3HT on glass and ZnO indicates that the presence of the ZnO acceptor did not produce additional polaron signals, which is in agreement with time-resolved microwave conductivity (TRMC) work by Piris et al, who also did not observe additional free carrier signals in P3HT/$Zn_{1-x}Mg_xO$ composites[65] (see Figure 6). ZnO and $Zn_{1-x}Mg_xO$ behave similarly as the electron acceptor because at low Mg concentration, Mg atoms substitute for Zn in the cation sites, and $Zn_{1-x}Mg_xO$ has the same wurtzite structure as ZnO. Hence, the conclusion drawn from the $Zn_{1-x}Mg_xO$ surface would apply to ZnO. Both the TRMC results and the TPA data presented here suggest that ZnO does not provide an exciton dissociation interface (Figure 6c) but instead functions as an electron-collecting medium for photoexcited charges dissociated in the P3HT layer (Figure 6b).

Whether ZnO provides an exciton dissociation interface is still unresolved, as experimental evidence exists for both sides. In the literature, it was argued that the ZnO/P3HT interface is efficient in dissociating excitons based on the magnitude of EQE.[30] Furthermore, if excitons are only dissociated in the polymer film and not at the ZnO/P3HT interface and carriers are collected due to the work function difference between ZnO and Ag, a metal electrode with a work function similar to that of ZnO should yield similar device performance. Single-layer organic photovoltaic devices are capable of high open-circuit voltage (>1 V) but produce very low J_{sc}.[66] Consequently, the highest performing devices yield a maximum EQE of ~1% or a J_{sc} of ~50 μA/cm^2 for single wavelength illumination.[67] The J_{sc} measured in ZnO/P3HT bilayer solar cells is one to two orders of magnitude larger than that of an equivalent device where the ZnO layer is omitted. A recent publication on solar cells made of a P3HT/ZnO blend formed from a ZnO precursor exhibit 50% internal quantum efficiency,[68] which is higher than the polaron generation rate in P3HT.[62] In addition, spectrally resolved photoinduced absorption data taken at steady state (microsecond time scale) clearly show a polaron peak in P3HT/ZnO nanoparticle composites.[30,68] The differences in the picosecond and microsecond TPA are two-fold: the peak power used in the excitation is many orders of magnitude higher in the picosecond experiment, and the millisecond experiments were performed at cryogenic temperatures to increase signal to noise. Since the time scale for the two experiments differs by several orders of magnitude and the low-temperature experiment substantially minimizes thermal effects on recombination, more experiments are needed to conclusively resolve the role of ZnO in hybrid solar cells.

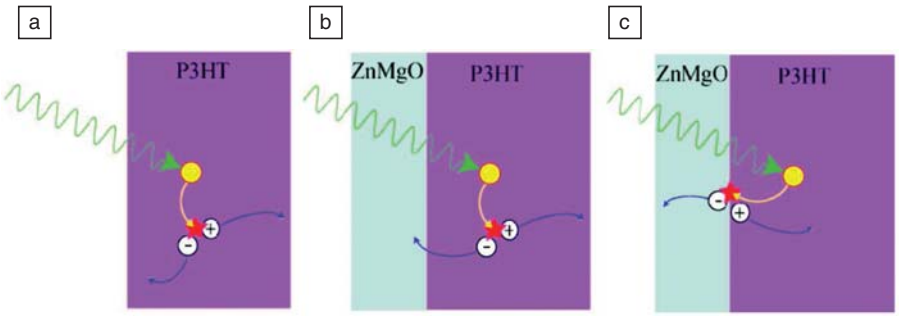

Figure 6. (a) Exciton dissociation within bulk P3HT. (b) Exciton dissociation within bulk P3HT followed by electron collection by the metal oxide layer. (c) Exciton dissociation induced by the P3HT/metal oxide interface followed by electron injection into the metal oxide layer. Reprinted with permission from Reference 43. ©2007, Wiley.

Summary

In summary, the interaction of the polymer with the substrate can substantially change the morphology at the interface. The structural changes in the interfacial polymer layer at the donor-acceptor interface are not evident when examining the bulk properties (e.g., UV-vis absorption or x-ray diffraction) of the thick layers employed in the solar cells. These changes manifest when measuring the action spectra of photoresponses (e.g., external quantum efficiency[30] or time-resolved microwave conductivity[65]) or using thin polymer films to model the interfacial layer. This is because the photoresponse is primarily generated near the heterojunction interface due to the short exciton or electron diffusion length in P3HT.

Due to the strong interaction between ZnO and the thiophene groups in P3HT, an amorphous interfacial polymer layer was formed that exhibits reduced exciton and polaron lifetimes. However, this polymer-substrate interaction can be mitigated using a self-assembled monolayer, consequently restoring the ordering of P3HT. Experimental results show that the ordering of P3HT at the donor-acceptor interface is critical in determining the recombination of photoexcited states. Better ordering leads to longer lifetimes and enhanced photocurrent and device efficiency.

Acknowledgments

The authors are grateful for the work conducted at Sandia, a multi-program laboratory operated by Sandia Corporation, a Lockheed Martin Company, for the United States Department of Energy's National Nuclear Security Administration under Contract DE-AC04-94AL85000.

References

1. C.J. Brabec, J. Durrant, *MRS Bull*. **33**, 670 (2008).
2. C.J. Brabec, J.A. Hauch, P. Schilinsky, C. Waldauf, *MRS Bull*. **30**, 50 (2005).
3. G. Li, V. Shrotriya, J. Huang, Y. Yao, T. Moriarty, K. Emery, Y. Yang, *Nat. Mater*. **4**, 864 (2005).
4. Y. Kim, S. Cook, S. Tuladhar, S. Choulis, J. Nelson, J. Durrant, D. Bradley, M. Giles, I. Mcculloch, C. Ha, M. Ree, *Nat. Mater*. **5**, 197 (2006).
5. J.Y. Kim, S.H. Kim, H. Lee, K. Lee, W. Ma, X. Gong, A. Heeger, *Adv. Mater*. **18**, 572 (2006).
6. Y. Liang, Z. Xu, J. Xia, S.-T. Tsai, Y. Wu, G. Li, C. Ray, L. Yu, *Adv. Mater.* 2010. DOI: 10.1002/adma.200903528.
7. X.W. Sun, J.Z. Huang, J.X. Wang, Z. Xu, *Nano Lett*. **8**, 1219 (2008).
8. S. Blumstengel, S. Sadofev, F. Henneberger, *New Journal of Physics* **10**, 065010 (2008).
9. J.B. Baxter, E.S. Aydil, *Appl. Phys. Lett*. **86**, 053114 (2005).
10. A.I. Hochbaum, P. Yang, *Chem Rev*. **110**, 527 (2010).
11. S. Hau, H. Yip, N. Baek, J. Zou, K. O'Malley, A. Jen, *Appl. Phys. Lett*. **92**, 253301 (2008).
12. F.C. Krebs, *Sol. Energy Mater. Sol. Cells* **92**, 715 (2008).
13. C. Li, T. Wen, T. Lee, T. Guo, J. Huang, Y. Lin, Y. Hsu, *J. Mater. Chem*. **19**, 1643 (2009).
14. M.T. Lloyd, D.C. Olson, P. Lu, E. Fang, D.L. Moore, M.S. White, M.O. Reese, D.S. Ginley, J.W.P. Hsu, *J. Mater. Chem*. **19**, 7638 (2009).
15. D. Olson, S. Shaheen, M. White, W. Mitchell, M. van Hest, R. Collins, D. Ginley, *Adv. Funct. Mater*. **17**, 264 (2007).
16. M.T. Lloyd, Y.-J. Lee, R.J. Davis, E. Fang, R.M. Fleming, R.J. Kline, M.F. Toney, J.W.P. Hsu, *J. Phys. Chem. C* **113**, 17608 (2009).
17. K.M. Coakley, M.D. McGehee, *Appl. Phys. Lett*. **83**, 3380 (2003).
18. D. Olson, J. Piris, R. Collins, S. Shaheen, D. Ginley, *Thin Solid Films* **496**, 26 (2006).
19. W.I. Park, D.H. Kim, S.W. Jung, G.-C. Yi, *Appl. Phys. Lett*. **80**, 4232 (2002).
20. W.L. Hughes, Z.L. Wang, *Appl. Phys. Lett*. **86**, 043106 (2005).
21. Y.W. Heo, V. Varadarajan, M. Kaufman, K. Kim, D.P. Norton, F. Ren, P.H. Fleming, *Appl. Phys. Lett*. **81**, 3046 (2002).

22. L. Vayssieres, K. Keis, S.-E. Lindquist, A. Hagfeldt, *J. Phys. Chem. B* **105**, 3350 (2001).
23. Z.R. Tian, J.A. Voigt, J. Liu, B. McKenzie, M.J. McDermott, M.A. Rodriguez, H. Konishi, H. Xu, *Nat. Mater*. **2**, 821 (2003).
24. R.B. Peterson, C.L. Fields, B.A. Gregg, *Langmuir* **20**, 5114 (2004).
25. L.E. Greene, M. Law, D.H. Tan, M. Montano, J. Goldberger, G. Somorjai, P. Yang, *Nano Lett*. **5**, 1231 (2005).
26. W.J. Beek, M.M. Wienk, M. Kemerink, X.N. Yang, R.A. Janssen, *J. Phys. Chem B* **109**, 9505 (2005).
27. A. Bashir, P.H. Wobkenberg, J. Smith, J.M. Ball, G. Adamopoulos, D.D.C. Bradley, T.D. Anthopoulos, *Adv. Mater*. **21**, 2226 (2009).
28. W.J.E. Beek, L.H. Slooff, M.M. Wienk, J.M. Kroon, R.A. Janssen, *Adv. Func. Mater*. **15**, 1703 (2005).
29. D.J.D. Moet, L.J.A. Koster, B. de Boer, P.W.M. Blom, *Chem. Mat*. **19**, 5856 (2007).
30. W.J.E. Beek, M.M. Wienk, R.A.J. Janssen, *Adv. Funct. Mater*. **16**, 1112 (2006).
31. E.L. Ratcliff, J.L. Jenkins, K. Nebesny, N.R. Armstrong, *Chem. Mater*. **20**, 5796 (2008).
32. S. Tong, C. Zhang, C. Jiang, Q. Ling, E. Kang, D. Chan, C. Zhu, *Appl. Phys. Lett*. **93**, 043304 (2008).
33. T. Monson, M. Lloyd, D. Olson, Y. Lee, J. Hsu, *Adv. Mater*. **20**, 4755 (2008).
34. C. Goh, S.R. Scully, M.D. McGehee, *J. Appl. Phys*. **101**, 114503 (2007).
35. S. Hau, H.-L. Yip, H. Ma, A. Jen, *Appl. Phys. Lett*. **93**, 233304 (2008).
36. E.D. Spoerke, M.T. Lloyd, E.S. Martin, D.C. Olson, Y.-J. Lee, J.W.P. Hsu, *Appl. Phys. Lett*. **95**, 213506 (2009).
37. L. Greene, M. Law, B.D. Yuhas, P. Yang, *J. Phys. Chem. C* **111**, 18451 (2007).
38. Y. Lin, T. Chu, C. Chen, W. Su, *Appl. Phys. Lett*. **92**, 053312 (2008).
39. P. Ravirajan, A.M. Peiro, M.K. Nazeeruddin, M. Graetzel, D.D.C. Bradley, J.R. Durrant, J. Nelson, *J. Phys. Chem. B* **110**, 7635 (2006).
40. Y.-Y. Lin, Y.-Y. Lee, L. Chang, J.-J. Wu, C.-W. Chen, *Appl. Phys. Lett*. **94**, 063308 (2009).
41. H. Sirringhaus, P.J. Brown, R.H. Friend, M.M. Nielsen, K. Bechgaard, B.M.W. Langeveld-Voss, A.J.H. Spiering, R.A.J. Janssen, E.W. Meijer, P. Herwig, D.M. de Leeuw, *Nature* **401**, 685 (1999).
42. G. Wang, J. Swensen, D. Moses, A.J. Heeger, *J. Appl. Phys*. **93**, 6137 (2003).
43. S. Cho, K. Lee, J. Yuen, G. Wang, D. Moses, A.J. Heeger, M. Surin, R. Lazzaroni, *J. Appl. Phys*. **100**, 114503 (2006).
44. R.J. Kline, M.D. McGehee, E.N. Kadnikova, J. Liu, J.M.J. Frechet, *Adv. Mater*. **15**, 1519 (2003).
45. Y. Kim, S. Cook, S.M. Tuladhar, S.A. Choulis, J. Nelson, J.R. Durrant, D.D.C. Bradley, M. Giles, I. McCulloch, C.-S. Ha, M. Ree, *Nat. Mater*. **5**, 197 (2006).
46. J.-F. Chang, B. Sun, D.W. Breiby, M.M. Nielsen, T.I. Solling, M. Giles, I. McCulloch, H. Sirringhaus, *Chem. Mater*. **16**, 4772 (2004).
47. W. Ma, C. Yang, X. Gong, K. Lee, A.J. Heeger, *Adv. Func. Mater*. **15**, 1617 (2005).
48. G. Li, V. Shrotriya, J. Huang, Y. Yao, T. Moriarty, K. Emery, Y. Yang, *Nat. Mater*. **4**, 864 (2005).
49. D. DeLongchamp, B.M. Vogel, Y. Jung, M.C. Gurau, C.A. Richter, Ol A. Kirillov, J. Obrzut, D.A. Fischer, S. Sambasivan, L.J. Richter, E.K. Lin, *Chem. Mater*. **17**, 5610 (2005).
50. R.J. Kline, D.M. DeLongchamp, D.A. Fischer, E.K. Lin, M. Heeney, I. McCulloch, M.F. Toney, *Appl. Phys. Lett*. **90**, 062117 (2007).
51. M.T. Lloyd, R.P. Prasankumar, M.B. Sinclair, A.C. Mayer, D.C. Olson, J.W.P. Hsu, *J. Mater. Chem*. **19**, 4609 (2009).
52. P.A.C. Quist, W. Beek, M. Wienk, R.A.J. Janssen, L.D.A. Siebbeles, *J. Phys. Chem. B* **110**, 10315 (2006).
53. J. Veres, S. Ogier, G. Lloyd, D.M. de Leeuw, *Chem. Mater*. **16**, 4543 (2004).
54. R.J. Kline, M.D. Mcgehee, M.F. Toney, *Nat. Mater*. **5**, 222 (2006).
55. F. Spano, *J. Chem. Phys*. **122**, 234701 (2005).
56. O. Inganas, W.R. Salaneck, J.-E. Osterhom, J. Laakso, *Synth. Met*. **22**, 395 (1988).
57. P.J. Brown, D.S. Thomas, A. Kohler, J.S. Wilson, J.-S. Kim, C.M. Ramsdale, H. Sirringhaus, R.H. Friend, *Phys. Rev. B* **16**, 064203 (2003).
58. J. Clark, C. Silva, R.H. Friend, F.C. Spano, *Phys. Rev. Lett*. **98**, 206406 (2007).
59. H.H. Yang, S.W. LeFevre, C.Y. Ryu, Z.N. Bao, *Appl. Phys. Lett*. **90**, 172116 (2007).
60. D.R. Lide, Ed., *Handbook of Chemistry and Physics, 84th Edition* (Boca Rotan, FL, 2003), Vol. Section 9, pp. 52–64.
61. J. Peet, J. Kim, N. Coates, W. Ma, D. Moses, A. Heeger, G. Bazan, *Nat. Mater*. **6**, 497 (2007).
62. C.X. Sheng, M. Tong, S. Singh, Z.V. Vardeny, *Phys. Rev. B* **75**, 085206 (2007).
63. R. Osterbacka, C.P. An, X.M. Jiang, Z.V. Vardeny, *Science* **287**, 839 (2000).
64. X. Ai, N. Anderson, J.C. Guo, J. Kowalik, L.M. Tolbert, T.Q. Lian, *J. Phys. Chem. B* **110**, 25496 (2006).
65. J. Piris, N. Kopidakis, D.C. Olson, S.E. Shaheen, D.S. Ginley, G. Rumbles, *Adv. Funct. Mater*. **17**, 3849 (2007).
66. G.G. Malliaras, J.R. Salem, P.J. Brock, J.C. Scott, *J. Appl. Phys*. **84**, 1583 (1998).
67. R.N. Marks, J.J.M. Halls, D.D.C. Bradley, R.H. Friend, A.B. Holmes, *J. Phys. Condens. Mater*. **6**, 1379 (1994).
68. S.D. Oosterhout, M.M. Wienk, S.S. v. Bavel, R. Thiedmann, L.J.A. Koster, J. Gilot, J. Loos, V. Schmidt, R.A.J. Janssen, *Nat. Mater*. **8**, 1 (2009). □

PARTICLE ACCELERATOR SYSTEMS

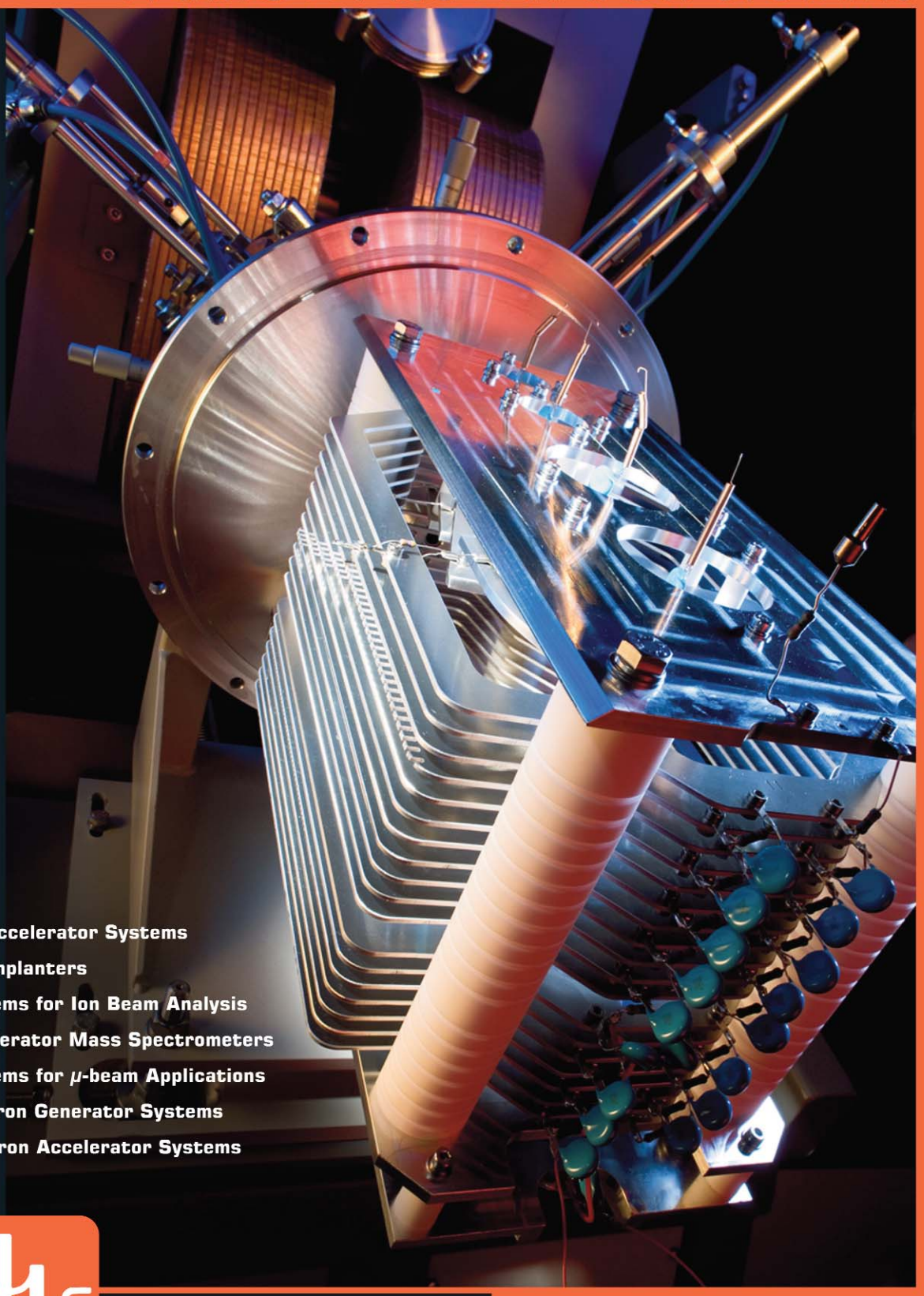

- Ion Accelerator Systems
- Ion Implanters
- Systems for Ion Beam Analysis
- Accelerator Mass Spectrometers
- Systems for μ-beam Applications
- Neutron Generator Systems
- Electron Accelerator Systems

High Voltage Engineering

High Voltage Engineering Europa B.V.
P.O. Box 99, 3800 AB Amersfoort, The Netherlands
Tel: 31 33 4619741 • info@highvolteng.com
www.highvolteng.com